Computing the exchange interaction in electron scattering from polyatomic molecules

P. Čarsky,[1] R. Čurik,[1] F. A. Gianturco,[2,*] R. R. Lucchese,[3] and M. Polasek[4]
[1]*J. Heyrowsky Institute of Physical Chemistry, Academy of Sciences of the Czech Republic, 18223 Prague 8, Czech Republic*
[2]*Department of Chemistry, The University of Rome, Cittá Universitaria, 00185 Rome, Italy*
[3]*Department of Chemistry, Texas A&M University, College Station, Texas 77843-3255*
[4]*Institute of Physics, Silesian University, Opava, Czech Republic*
(Received 23 October 2000; revised manuscript received 21 November 2001; published 2 May 2002)

The treatment of the exchange potential between the bound electrons of a polyatomic target and the continuum electron from the impinging beam employed in single-collision scattering experiments is considered by using different computational approaches. In the relevant experimental setup the impinging electron undergoes single scattering with the gaseous target molecule and only the elastic channel is being considered by the present calculations. The chosen example of the benzene molecule shows that the various modeling of the all-important exchange interaction yield good agreement with the existing experiments and suggest that they could be profitably employed to analyze elastic angular distributions from polyatomic targets of fairly high complexity and fairly large number of bound electrons.

DOI: 10.1103/PhysRevA.65.052713 PACS number(s): 34.80.Bm, 33.20.−t

I. INTRODUCTION

Recent years have seen a rapid expansion of the technological applications of plasmas, particularly in the development of plasma reactors for semiconductor manufacturing. Furthermore, molecular plasmas also play a role, among other technologies, in the preparation of pollution control equipments and flat panel displays, just to cite a few examples [1].

The task of modeling the role of the various gases contained in the plasmas, and of the reaction products, is obviously essential for control, optimization, and development purposes. The assembly of such models, therefore, requires knowledge of the basic collision processes that occur in the plasma and at the plasma-wafer interface: the majority of these processes are initiated by electron scattering [2]. There is therefore a real need for information on elastic and inelastic cross sections involving the relevant plasma reagent and product molecules, fragmentation dynamics, dissociative attachment, and ionization for both the primary components and its fragments or reaction products [3]. The knowledge required includes not only data characterizing individual collisions but also the assembly of corresponding theoretical and computational models that are not excessively demanding on computer time and are numerically robust for repeatedly handling a broad variety of systems.

Cross sections are essentially a measure of the probability for a given dynamical process to occur and therefore our understanding of the macroscopic behavior inevitably depends upon our understanding of the microscopic details of the collisional events. On the other hand, either the measured or the computed data are fairly few and far apart on the energy scale and on the range of properties examined, hence the demand on more extended and detailed information [4,5].

*Corresponding author. FAX: +39-6-49913305. Email address: FAGIANT@CASPUR.IT

Any quantum treatment of the elementary electron-molecule collision requires beforehand an accurate and realistic description of the forces at play, especially when the gaseous molecules become increasingly larger in terms of number of electrons and nuclei bound within them. One of the more difficult terms of that interaction comes from the existence of strong exchange forces between the bound molecular electrons and the impinging continuum electron [6].

The aim of the present study is therefore to use two different ways of handling such interaction effects for a specific polyatomic molecule that also has relevance for plasma modeling studies [4]: the gaseous benzene molecule. Since the main focus of this work is on assessing the reliability of the methods with respect to the existing experiments, we will test our results by comparing computed and measured angular distributions over a range of collision energies. We will also compare our results with other, earlier calculations on the same system [7]. The paper is organized as follows: the following Sec. II briefly describes the general scattering equations, while Sec. III reports more in detail our different treatments of the exchange interactions. The results obtained for C_6H_6, their comparison with experiments and with previous calculations are reported in Sec. IV, while Sec. V summarizes our conclusions.

II. THE SCATTERING EQUATIONS

A. Single-center expansions

Resonant and nonresonant low-energy scattering of electrons from polyatomic targets can be studied theoretically (and computationally) at various levels of description: (i) of the electronuclear structure of the target molecule, (ii) of the interaction forces between the bound particles and the impinging electron, and (iii) of the dynamical formulation of the quantum-scattering equations [8].

Within an *ab initio*, parameter-free approach one could start with the target nuclei being kept fixed at their equilibrium geometry and their motion during the scattering process

could then be decoupled from the other variables. The simplifying scheme goes under the familiar name of the fixed nuclei approximation [6] and it greatly reduces the dimensionality of the coupled scattering equations for the dynamics. In our implementation of the scattering equations any arbitrary three-dimensional function describing a given electron is obtained around a single center of expansion (SCE) usually taken to be the center of mass of the global $(N+1)$ electron molecular structure

$$F^{p\mu}(r,\hat{\mathbf{r}}|\mathbf{R})=\sum_{l,h} r^{-1} f_{lh}^{p\mu}(r|\mathbf{R}) X_{lh}^{p\mu}(\hat{\mathbf{r}}). \tag{1}$$

In the above SCE representation $F^{p\mu}$ refers to the μth element of the pth irreducible representation (IR) of the point group of the molecule at the nuclear geometry $\mathbf{R}$. The angular functions $X_{lh}^{p\mu}(\hat{\mathbf{r}})$ are symmetry adapted angular functions given by proper combination of spherical harmonics $Y_{lm}(\hat{\mathbf{r}})$ [9].

The corresponding quantum-scattering equations will give us a way of evaluating the unknown radial coefficients of Eq. (1) for the $(N+1)$th continuum electron by using the SCE radial quantities for the occupied target molecular orbitals (MO's)

$$\left[\frac{d^2}{dr^2}-\frac{l(l+1)}{r^2}+2(E-\epsilon_\alpha)\right] f_{lh}^{p\mu\alpha}(r|\mathbf{R}) = 2\sum_{l'h'\beta}\int dr'\, V_{lh,l'h'}^{p\mu,\alpha\beta}(r,r'|\mathbf{R}) f_{l'h'}^{p\mu,\beta}(r'|\mathbf{R}), \tag{2}$$

where E is the collision energy $E=k^2/2$ and ϵ_α is the electronic eigenvalue for the αth asymptotic state. The $p\mu$ indices employed on the rhs of Eq. (2) label the specific μth component of the pth IR that belongs to the αth electronic target state (initial state) coupled to the of excited-state indexed by β. The coupled partial integro-differential equations (IDE's) (2), contain the kernel of the integral operator V, which is a sum of diagonal and nondiagonal terms that, in principle, can fully describe the electron-molecule interaction during the collision. The near-HF (Hartree-Fock) wave function from a single-determinant–self-consistent-field (SD-SCF) calculation can be used to represent the bound target electrons, thus reducing the sum of the rhs of Eq. (2) to a single state α only. This simplification obtains the static-exchange (SE) representation of the electron-molecule interaction for the chosen electronic target state (usually the ground state) at the nuclear geometry $\mathbf{R}$.

The numerical solutions of the coupled Eq. (2) produce the relevant K-matrix elements that in turn yield the differential cross sections for scattering by randomly oriented molecules after averaging the scattering amplitude $f(\hat{k}\cdot\hat{r}|\alpha,\beta,\gamma)$ over all the angular values [8]

$$\frac{d\sigma}{d\Omega}(\hat{k}\cdot\hat{r})=\frac{1}{8\pi^2}\int |f(\hat{k}\cdot\hat{r}|\alpha,\beta,\gamma)|^2 d\alpha\sin(\beta)d\beta\,d\gamma. \tag{3}$$

A more convenient formulation of the above quantity can be had by writing [6]

$$\frac{d\sigma}{d\Omega}(\hat{k}\cdot\hat{r})=\sum_L A_L P_L(\cos\vartheta), \tag{4}$$

with ϑ being now the center-of-mass (c.m.) angle from the impinging direction of $\hat{k}$. The coefficients A_L have been given explicitly before [9] and will not repeated here. The interested readers can refer to the above work for the details.

B. Interaction forces

For a target that has a closed-shell electronic structure, as in the present example, with $n_{\rm occ}$ doubly occupied orbitals φ_i and when only a single state is included in the expansion of Eq. (2), the potential is the static-exchange potential that has the form

$$V_{\rm ESE}(\mathbf{r})=\sum_{\gamma=1}^{M}\frac{Z_\gamma}{|\mathbf{r}-\mathbf{R}_\gamma|}+\sum_{i=1}^{\eta_{\rm occ}}(2\hat{J}_i-\hat{K}_i), \tag{5}$$

where $\hat{J}_i$ and $\hat{K}_i$ are the usual local static potential and the nonlocal exchange potential operators, respectively. The index γ labels one of the M nuclei located at the coordinate $\mathbf{R}_\gamma$ in the center of mass.

In the present work we intend to mainly discuss the case where the static interaction is combined with the exchange interaction only, thereby looking into the specific effects of different exchange terms on the final behavior of the differential cross sections (DCS) that shall thus be obtained within the exact-static-exchange (ESE) approximation. In order to see the effect of the missing interaction on the comparison between calculations and experiments, in a few cases, we will further include correlation-polarization effects following a global modeling employed already successfully by our group for the benzene target molecule [10] and which has been described in detail in our previous work on polyatomic molecular gases [6,9,10].

III. BOUND-CONTINUUM EXCHANGE INTERACTIONS

A. The discrete momentum representation

The variational treatments of electron-molecule collisions (see for example Refs. [8] or [11]) usually employs Gaussian-type functions as the variational basis set. Although the use of Gaussians in bound-state calculations has become a routine task, their utilization in scattering problems is not so simple. One needs a large set of diffuse functions to represent properly all the operators appearing in the variational functional. Moreover, the S-matrix Kohn method requires additional continuum functions with correct asymptotic behavior. The choice of the resulting set is connected with some uncertainty and may lead to linear dependence. For these reasons, it is desirable to separate basis functions used for the construction of the Hartree-Fock potential and those appearing in the solution of the scattering equations. The basic construction principle of using a best fit

of plane waves (e.g., see Refs. [12,13]) allows to express the Green's function in a separate form and to obtain *T*-matrix elements by simple inversion of the Lippmann-Schwinger equation. Unfortunately, this method suffers from two main disadvantages: without semiempirical adjustment it yields infinite diagonal elements of the Green's function, and its interaction potential matrix becomes nearly singular at lower energies.

To overcome these problems, a numerical quadrature in **k** space has been recently proposed [14] to solve the corresponding Lippmann-Schwinger equation. To stress the formal analogy with the discrete variable representation, the method was called the discrete momentum representation (DMR) method. It leads to a matrix equation for scattering amplitudes similar to that in the *T*-matrix expansion [11] and the discrete of quadrature vectors in the **k** space may be considered as a basis set that represents the *T*-operator matrix once the molecular potential is available in any standard basis set.

The essence of the method, already described in Ref. [14], is to perform a numerical quadrature of the UGT term in the Lippmann-Schwinger equation

$$\hat{T}=\hat{U}+\hat{U}\hat{G}\hat{T}, \tag{6}$$

which, in momentum representation, has the form

$$\langle \mathbf{k}_1|\hat{T}|\mathbf{k}_2\rangle=\langle \mathbf{k}_1|\hat{U}|\mathbf{k}_2\rangle+\int d\mathbf{k}\frac{\langle \mathbf{k}_1|\hat{U}|\mathbf{k}\rangle\langle \mathbf{k}|\hat{T}|\mathbf{k}_2\rangle}{k_0^2-k^2+i\epsilon}. \tag{7}$$

The numerical quadrature of the integral on the rhs of the equation (7) converts the operator equation (6) into the matrix equation

$$T_{ij}=U_{ij}+\sum_k U_{ik}G_{kk}T_{kj} \tag{8}$$

and, after the matrix inversion, to the working equation

$$\mathbf{T}=(1-\mathbf{UG})^{-1}\mathbf{U}. \tag{9}$$

U is twice the static-exchange potential, and *i*, *j*, and *k* are indices for the roots of the numerical quadrature. The integration range from zero to infinity for the integration in the momentum space was first cutoff to finite maximum momenta and then transformed to the integration interval $\langle -1, 1\rangle$ using the transformation formula

$$x=\frac{a(k-k_0)}{b(k+k_0)}, \tag{10}$$

where k_0 corresponds to the energy of the incident electron, and a and *b* are adjustable parameters that define the integration interval in the momentum space.

A special feature of the DMR method is that it yields differential cross sections for scattering angles given by **k** vectors contained in the numerical quadrature set. Differential cross sections for any other scattering angle is obtained by interpolation. The interpolation formula has also been used for molecular geometry averaging [15].

In the results discussed in the following section, the outcomes of the present calculations will be labeled as the DMR-SE treatment of the collisional event.

B. The iterative exchange approach

In the SCE expansion described in Sec. II all functions are written as

$$f(r,\theta,\phi)=\sum_{l,m} f_{lm}(r)\mathbf{Y}_{lm}(\theta,\phi). \tag{11}$$

The product of such two functions could be given by first transforming the angular-momentum representation of *f* into a coordinate representation using

$$f_{\alpha,\beta}(\mathbf{r})=\sum_{l,m} f_{lm}(\mathbf{r})\mathbf{U}_{lm,\alpha,\beta}, \tag{12}$$

where $U_{lm,\alpha,\beta}=Y_{lm}(\theta_\alpha,\phi_\beta)$ and $f_{\alpha,\beta}(\mathbf{r})=f(r,\theta_\alpha,\phi_\beta)$. In this representation a product of two functions is just a point-by-point product of the form [16]

$$(f\cdot g)_{\alpha\beta}(\mathbf{r})=f_{\alpha\beta}(\mathbf{r})\mathbf{g}_{\alpha\beta}(\mathbf{r}). \tag{13}$$

The angular-momentum representation can then be recovered by transforming back from the coordinate representation

$$f_{lm}(\mathbf{r})=\sum_{\alpha\beta} f_{\alpha,\beta}(\mathbf{r})\mathbf{V}_{\alpha\beta}, \tag{14}$$

where

$$\mathbf{V}_{\alpha\beta,lm}=\mathbf{Y}_{lm}(\theta_\alpha\phi_\beta)\mathbf{W}_\alpha\mathbf{W'}_\beta. \tag{15}$$

The evaluation of the transformation given by Eq. (12) depends only on the second power of the number of partial waves and therefore can significantly reduce the effort needed to evaluate the nonlocal part of the bound-continuum interaction. One has to evaluate the exchange integrals between bound and continuum electrons

$$\sum_\alpha \int \phi_\alpha(\mathbf{r}')|\mathbf{r}-\mathbf{r}'|^{-1}\mathbf{F}^{(p\mu)}(\mathbf{r}')d\mathbf{r}'\,\phi_\alpha(\mathbf{r}), \tag{16}$$

where α sums over the occupied target MO's given by the ϕ_α functions and the $\mathbf{F}^{(p\mu)}$ are the continuum electron functions for any IR labeled by the $|p\mu\rangle$ indices mentioned earlier. The procedure involves generating iteratively the orbitals $F^{(p\mu)}$ until convergence is achieved for the structure of the elements of the scattering *K* matrix, within a given threshold of invariance for all of them (usually about 0.1%). One can further improve on the convergence of the iterative method by taking advantage of the Schwinger variational treatment [17]. The equation are then rewritten in terms of a

Lippmann-Schwinger equation and the details of the method have been reported before [17,18]

The corresponding *K*-matrix elements can then be used to evaluate total integral cross sections (rotationally summed) and further employed to generate differential cross sections (DCS) for the elastic process, as we shall show with the results given below. It will be called the SCE-SE treatment of the scattering process.

IV. COMPUTED DIFFERENTIAL CROSS SECTIONS

To evaluate both the static potential and the exchange interaction in the SCE expansion discussed before, we expanded first around the molecular center of mass the Gaussian functions employed to represent the target electrons. They were given by the following. (i) Triple-zeta-valence basis set plus two polarization functions on each atomic center. The molecular geometry used $R_{\text{C-C}}=1.397$ Å and $R_{\text{C-H}}=1.084$ Å. This basis set was obtained through the CADPAC set of codes [20]. (ii) Double-zeta-valence basis set of Dunning and Hay [21] with 66 basis functions at the optimized geometry of $R_{\text{C-C}}=1.397$ Å and $R_{\text{C-H}}=1.073$ Å, yielding a total Hartree-Fock energy of $-230.641\,65$ hartrees. Both basis sets for the description of the molecular bound states appeared to give exactly the same differential cross sections and therefore only one set of results will be given.

The partial-wave expansion for both the continuum electron and the SE interaction was carried out up to $l_{\max}=40$. When we further added correlation-polarization (CP) effects, V_{CP} the asymptotic dipole polarizability value that we employed was of $69.64a_0^3$, evenly divided between the six carbon centers as we had done before [10]. The matching radius with the inner correlation term given via density-functional theory was $7.712a_0$ [10]. The radial integration for the coupled IDE of Eq. (2) was extended to 1336 points and the (θ,φ) integration involved (84×81) points, reduced within each IR by the symmetry requirements. The computational time was of 0.3 h for the orbital expansion, 16.6 h for all symmetry contributions to scattering at one energy, and 8.7 h for DCS evaluation. The work was carried out on a SGI *R*10 000, 200-MHz workstation.

In the DMR calculations the target wave function was described by the valence double-zeta basis set of Dunning and Hay [21]. The density matrix of the electronic distribution obtained for the optimized geometry was stored to provide the input for the DMR calculations that generated first the Coulomb and exchange integrals of the SE treatment discussed earlier. The constants *a* and *b* in Eq. (10) were set to $a=10.333$ and $b=9.667$, which corresponds to the momentum range from $0.033k_0$ to $30k_0$. A Gauss-Legendre quadrature was employed for the radial integration and a Lebedev quadrature handled the angular integration. The number of points used in the angular quadrature was 974 and the number of points in the radial quadrature was increased stepwise to check the convergence. The DCS's obtained for four highest and computationally feasible radial quadratures were averaged and the range scanned by the respective four DCS's for a given energy and scattering angle was taken as an estimated error. Each calculation at one energy took 11 h for the static interaction and 13 h for the exchange interaction. The inversion of the Lippman-Schwinger equation took 4 h, for a total of 28 h for one energy and 181 points for each DCS. The work was carried out on a PC-Pentium III.

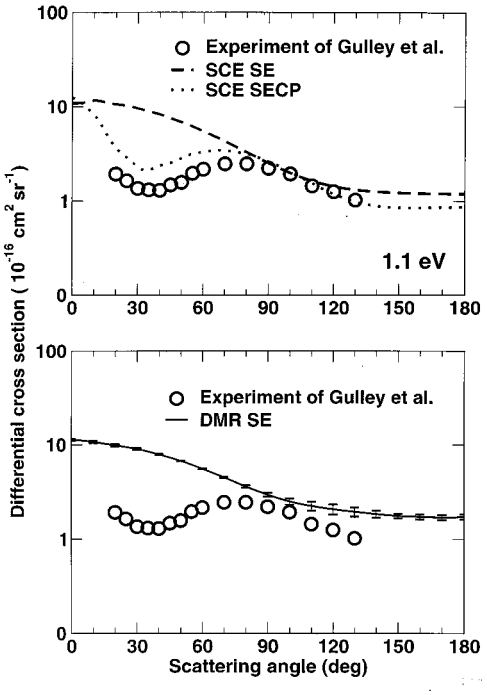

FIG. 1. Computed and measured angular distributions for electron scattering from gaseous benzene for the collision energy of 1.1 eV. The open circles show the experiments from Ref. [23]. Upper panel: the dashed line is the static-exchange calculation with the iterative method (SCE) while the dotted line was obtained from the calculation that included correlation-polarization effects within the SCE method. Lower panel: an average from discrete momentum representation calculations performed with radial numerical quadratures with 29, 31, 33, and 37 points. The error bars were estimated as described in the text.

The results of calculations are presented in Figs. 1–6, showing the angular dependence of observed and calculated DCS at 1.1, 4.9, 10, 15, 20, and 30 eV. In the upper panels, we present reference calculations and in lower panels, we present DMR DCS's with the estimated error bars. For the low-energy regime at 1.1 and 4.9 eV we show two sets of reference calculations: (i) the SE calculations that employ the iterative exchange scheme (SCE-SE), and (ii) the SCE calculations that further include the global correlation polarization, V_{CP} potential employed in our earlier work [19] and in our recent calculations on the benzene molecule [22] (SCE-SECP). At the lower energy 1.1 eV, one clearly sees that the inclusion of correlation-polarization effects has a marked effect on the computed angular distributions and is important to improve their agreement with the measured data [22].

When one moves to the higher collision energy, on the other hand (see Fig. 2), the V_{CP} contributions to the full electron-molecule interaction become less significant, showing there that both SE and SECP calculations for the DCS at 4.9 eV are very similar to each other and in good accord with

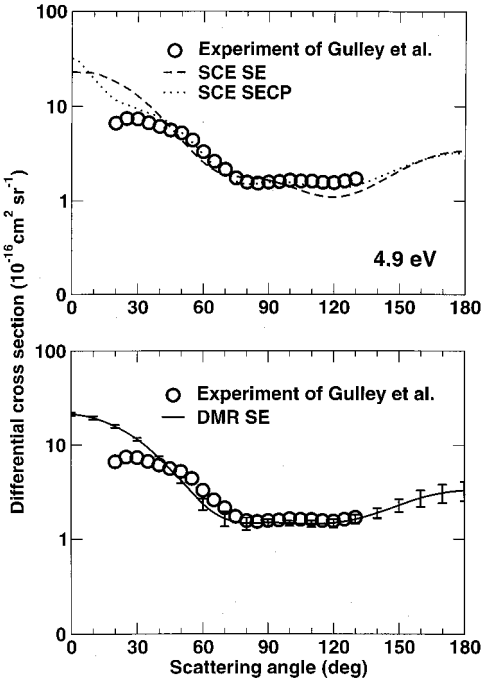

FIG. 2. Same quantities as in Fig. 1 but for the collision energy of 4.9 eV. The DMR line in the lower panel is an average from values obtained with radial quadratures containing 29, 31, 33, and 35 points.

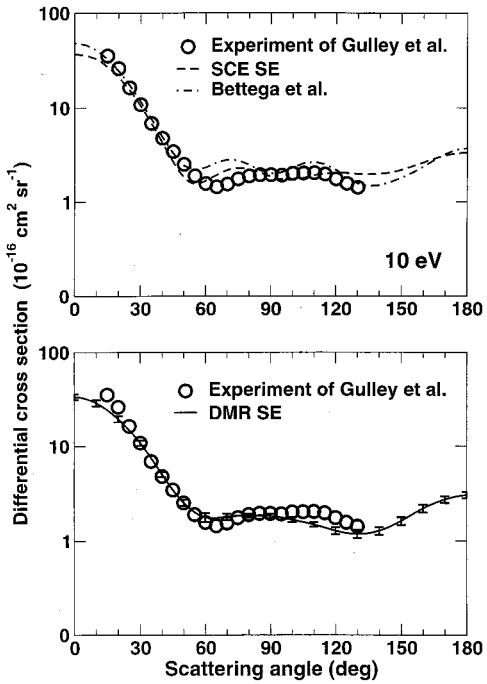

FIG. 3. Same as in Figs. 1 and 2 but for the collision energy of 10 eV. The dashed line in the upper panel is the SCE calculation. The upper panel also shows the computed SE values (dot-dashed line) using the SMC approach from Ref. [7]. See Fig. 1 for the meaning of other symbols. The DMR line in the lower panel is an average from values obtained with radial quadratures containing 23, 25, 27, and 29 points.

experiments. It is also significant to note that, at both the energies of 1.1 and 4.9 eV, the SCE and DMR calculations at the static and exchange level are essentially coincident.

The comparison between measured and computed differential cross sections is extended to higher collision energies by the results reported in Figs. 3–6. In Figs. 3 and 4, we present the measured angular distributions at 10 and 15 eV, also from Ref. [23] and both sets of our calculations at the SE level, using the SCE and DMR methods discussed in the previous sections. The corresponding SCE calculations at the SECP level were not reported because they essentially coincide with the points from the SCE-SE calculations. We further report in the two figures the results from another set of independent calculations recently carried out on the same system [7]. Those calculations employed the Schwinger multichannel method (SMC) described in detail in their earlier work [24,25]. The general physical modeling of the dynamics was the same of ours (fixed nuclei, SE, and SECP interactions) and both the occupied and scattering orbitals were described through a 6-311++G $(2d,p)$ basis set internal to the electronic structure program GAMESS [26].

It is clear from the shown comparison between theoretical results and the experimental findings that all the calculated values follow the experiments remarkably closely in the small-angle region ($\vartheta_{\text{c.m.}} \leqslant 60°$) while departing from measurements at the larger angles. We also see that the SCE and DMR results differ from each other in the large-angle scattering, with the DMR results following better the experimental oscillations.

As one moves to even higher collision energies, however, all theoretical results at the SE level turn out to be coincident

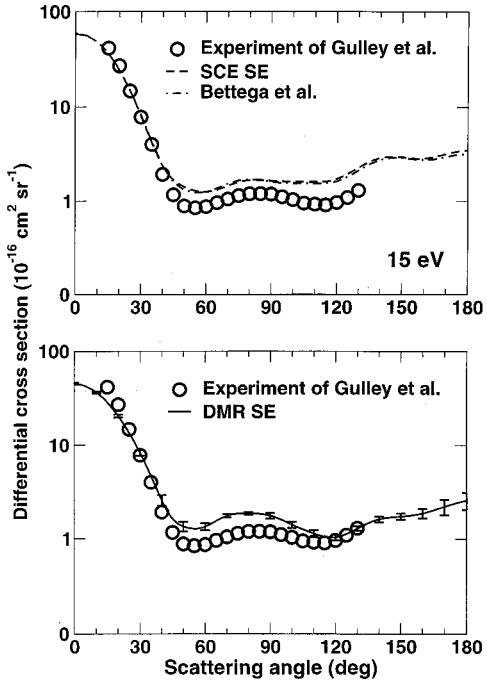

FIG. 4. Same as in Fig. 3 but for the collision energy of 15 eV. The DMR line in the lower panel is an average from values obtained with radial quadratures containing 21, 23, 25, and 27 points.

with each other, as seen by the results presented in Figs. 5 and 6. We show there the measured results at 20 and 30 eV [23] and also both the present calculations and those from Ref. [7]. All the calculations follow very well experiments up to $\vartheta_{\text{c.m.}} \sim 60°$ and reproduce reasonably well the flat, slowly oscillating angular distributions between $\vartheta_{\text{c.m.}} \sim 60°$ and 120°, while however giving larger DCS values in that angular region for both collision energies. Furthermore, the SCE and SMC computed quantities agree well with each other in the backscattering region up to $\vartheta_{\text{c.m.}} \sim 180°$, while the DMR results show larger values in the extreme backscattering region for the collision energy of 30 eV (see Fig. 6).

As it can be seen from Figs. 1–6, at least a part of the discrepancy between the iterative SCE and DMR results, in particular for large scattering angles, may be assigned to the errors of DMR calculations caused by a slow convergence of the numerical quadrature. Most probably the error would be reduced by using a larger numerical quadrature. However, this would cause a considerable increase of the computational cost and the need of a more powerful workstation instead of a Pentium PC as done here. It would thus be more profitable to search for a more effective numerical quadrature: such work is already in progress and the preliminary results show that the slow convergence is due to the static potential term because of the long-range nature of the nuclear terms in momentum space and not due to the exchange contribution. As an example of this, Fig. 7 shows the convergence of calculated DCS when the interaction potential is limited to the exchange term only. One sees in that figure how good convergence is obtained already with very small Legendre quadratures, with the angular quadrature also converging rather fast. The number of points in the Lebedev quadrature, in fact, could be lowered from 974 to 194 angular points without any visible change in the solid line of Fig. 7.

On the whole, however, all three types of independent SE calculations agree well with each other over the whole set of examined energies and for most of the angular range at each energy. They are also close to the experimental findings

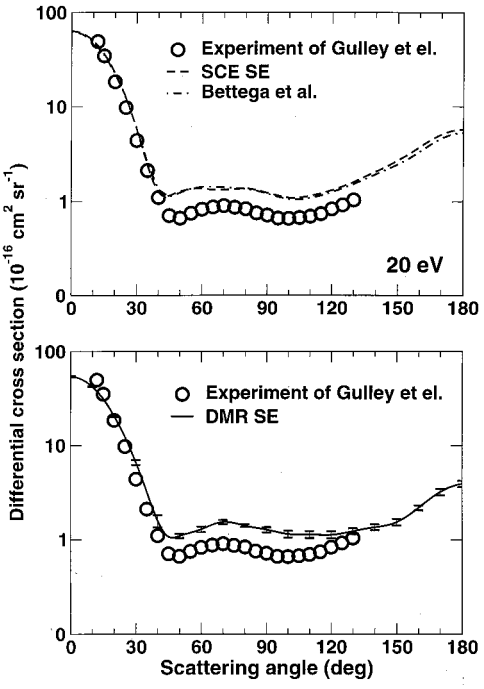

FIG. 5. Same as in Fig. 3 but for the collision energy of 20 eV. The DMR line in the lower panel is an average from values obtained with radial quadratures containing 15, 19, 21, and 23 points.

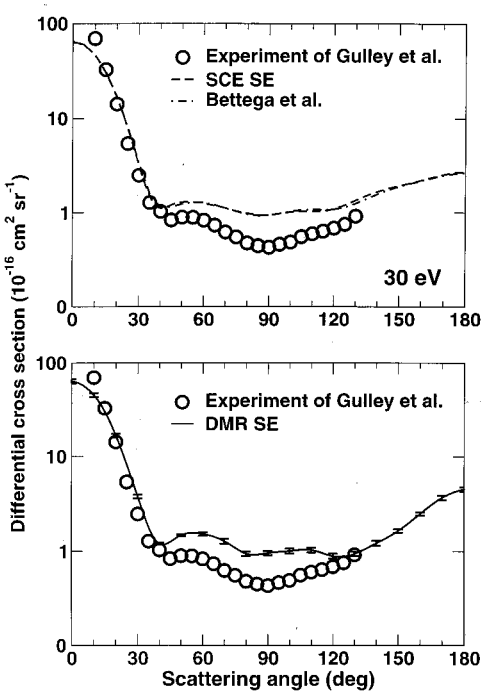

FIG. 6. Same as in Fig. 3 but for the collision energy of 30 eV. The DMR line in the lower panel is an average from values obtained with radial quadratures containing 17, 19, 21, and 23 points.

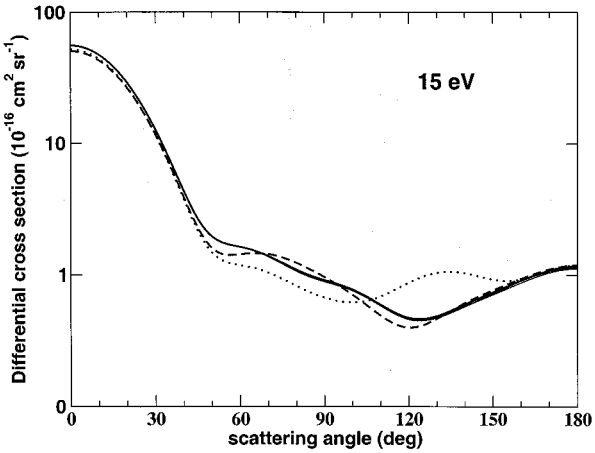

FIG. 7. Test of convergence of the radial quadrature for the exchange potential: computed angular dependence for electron scattering from benzene at the collision energy of 15 eV. The DMR calculations were performed with different numbers of radial points: 7 (dotted line), 9 (dashed); lines for 11, 13, 15, 17, 19, 21, 23, and 25 points coincide and they are all represented by a single solid line.

above about 4 eV and for all the energies computed here. The actual numerical values of the SCE, DMR, and SMC computed DCS are reported in the Appendix.

V. SUMMARY AND CONCLUSIONS

In our present work we have described two different, independent ways of evaluating *K*-matrix and *T*-matrix scattering elements for describing electron collisions of a fairly complex polyatomic target such as benzene and over a broad range of collision energies. In particular, we have verified once more that correlation-polarization effects are likely to play a minor role on the behavior of elastic angular distributions for collision energies above about 4–5 eV. Thus, a static-exchange description of elastic DCS is sufficient to bring computed values into quantitative agreement with available experiments, at least for elastic-scattering data. Furthermore, we have compared two different computational methods to handle the quantum dynamics, the SCE iterative method, and the DMR method and found them to give essentially the same results at all energies examined and also to give very good accord with experimental angular distributions. A further comparison with earlier calculations [7] also showed that their SE results are very close to the present ones.

In conclusion, therefore, we have found that at least two different computational paths can be followed to treat, efficiently and realistically, electron scattering from fairly large polyatomic targets and that both methods provide good accord, on an absolute scale, with experimental data of measured angular intensities for elastic scattering.

ACKNOWLEDGMENTS

The financial support of The Italian Ministry for Universities and Research (MURST) and of the Center for Supercomputing Applications (CASPUR) is gratefully acknowledged. F.A.G. and R.R.L. thank NATO organization for the award of a Collaborative Research Grant (Grant No. 950522). R.R.L. also thanks the Welsh Foundation for financial support (Grant No. A-1020). The support from the Grant Agency of the Czech Republic (Grant No. 203/99/0839) is also gratefully acknowledged. Finally, we all thank Professor S. J. Buckman for sending us the files with the experimental results and for useful correspondence about them.

APPENDIX

In this appendix, we present numerical data from Figs. 1–6 for selected scattering angles given in Table I. The SMC differential cross sections are taken from Ref. [7].

TABLE I. Angular dependence of the differential cross section for the elastic scattering by the benzene molecule for examined collision energies *E*.

	Differential cross section (Å^2)									
	Scattering angle									
Method	0°	20°	40°	60°	80°	100°	120°	140°	160°	180°
$E=1.1$ eV										
DMR	11.4	9.9	7.9	5.5	3.6	2.5	2.1	1.8	1.7	1.7
SCE	10.9	10.6	8.3	5.4	3.3	2.0	1.4	1.3	1.2	1.2
					$E=4.9$ eV					
DMR	21.3	15.8	7.3	2.4	1.5	1.5	1.5	1.9	2.8	2.3
SCE	22.9	22.3	7.9	2.5	1.7	1.4	1.1	1.6	2.7	3.4
					$E=10$ eV					
DMR	33.7	19.5	5.0	1.8	1.8	1.7	1.3	1.3	2.2	3.0
SCE	36.8	21.0	4.3	1.7	2.2	1.7	2.0	2.0	2.6	3.3
SMC	48.3	24.7	4.9	2.3	2.5	2.3	2.2	1.5	2.4	3.7
					$E=15$ eV					
DMR	45.2	20.4	2.6	1.3	1.9	1.4	1.0	1.6	1.9	2.6
SCE	58.2	24.3	2.4	1.3	1.7	1.6	1.7	2.9	2.8	3.4
SMC	59.4	24.8	2.4	1.3	1.7	1.6	1.6	2.8	2.7	3.2
					$E=20$ eV					
DMR	53.9	22.5	1.6	1.3	1.4	1.1	1.1	1.4	2.2	3.9
SCE	63.6	22.7	1.3	1.4	1.4	1.1	1.3	2.1	3.7	5.7
SMC	62.8	22.4	1.3	1.4	1.4	1.1	1.3	1.9	3.3	5.3
					$E=30$ eV					
DMR	63.7	16.7	1.2	1.5	0.9	1.0	0.9	1.2	2.5	4.5
SCE	63.5	16.6	1.1	1.2	1.0	1.0	1.1	1.7	2.2	2.7
SMC	65.2	17.1	1.1	1.3	1.0	1.0	1.1	1.6	2.2	2.6

[1] J. N. Bardsley, in *Abstracts of the International Conference on Atomic and Molecular Data and their Applications*, edited by W. L. Wiese (NIST, Washington, DC, 1997), p. 3.
[2] M. A. Ali, Y.-K. Kim, W. Hwang, N. M. Weinberger, and M. E. Rudd, J. Chem. Phys. **106**, 9602 (1997).
[3] J. E. Sanabia, G. D. Cooper, J. A. Tosell, and J. H. Moore, J. Chem. Phys. **108**, 389 (1998).
[4] L. G. Christophorou, J. K. Olthoff, and M. V. V. S. Rao, J. Phys. Chem. Ref. Data **25**, 1341 (1996).
[5] L. G. Christophorou, J. K. Olthoff, and M. V. V. S. Rao, J. Phys. Chem. Ref. Data **26**, 1 (1997).
[6] F. A. Gianturco and A. Jain, Phys. Rep. **143**, 347 (1986).
[7] M. H. F. Bettega, C. Winstead, and V. McKoy, J. Chem. Phys. **112**, 8806 (2000).
[8] *Computational Methods for Electron-Molecule Collisions*, edited by W. H. Huo and F. A. Gianturco (Plenum, New York, 1995).
[9] F. A. Gianturco and N. Sanna, Comput. Phys. Commun. **114**, 142 (1998).
[10] F. A. Gianturco and R. R. Lucchese, J. Chem. Phys. **108**, 6144 (1998).
[11] C. Winstead and V. McKoy, in *Modern Electronic Structure Theory*, edited by D. R. Yarkony (World Scientific, Singapore, 1995), Pt. II.
[12] P. Čársky, V. Hrouda, and J. Michl, Int. J. Quantum Chem. **53**, 419 (1999).
[13] P. Čársky, V. Hrouda, M. Polášek, D. E. David, D. Antic, and J. Michl, J. Phys. Chem. **101**, 3754 (1997).
[14] M. Polášek, M. Juřek, M. Ingr, P. Čársky, and J. Horáček, Phys. Rev. A **61**, 032701 (2000); M. Ingr, M. Polášek, P. Čársky, and J. Horáček, *ibid.* **62**, 032703 (2000).
[15] P. Čársky and M. Polášek (unpublished).
[16] R. R. Lucchese, J. Chem. Phys. **92**, 4203 (1990).
[17] C. Winstead and V. McKoy, Phys. Rev. A **42**, 5357 (1990).
[18] R. R. Lucchese and V. McKoy, Phys. Rev. A **42**, 5357 (1990).
[19] F. A. Gianturco, R. R. Lucchese, and N. Sanna, J. Chem. Phys. **102**, 5743 (1995).
[20] R. D. Amos and J. E. Rice, CADPAC: *The Cambridge Analitic Derivatives Package, Issue 5.2* (Cambridge University Press, Cambridge, 1993).
[21] T. M. Dunning and P. J. Hay, in *Modern Theoretical Chemistry*, edited by H. F. Schaefer, Jr. (Plenum, New York, 1977), Vol. 3.
[22] F. A. Gianturco and R. R. Lucchese, J. Chem. Phys. **113**, 10 044 (2000).
[23] R. J. Gulley and S. J. Buckman, J. Phys. B **32**, L405 (1999).
[24] K. Takatsuka and V. McKoy, Phys. Rev. A **24**, 2473 (1981).
[25] K. Takatsuka and V. McKoy, Phys. Rev. A **30**, 1734 (1984).
[26] M. W. Schmidt, K. K. Baldridge, J. A. Boatz, S. T. Elbert, M. S. Gordon, J. M. Jensen, S. Koseki, N. Matsunaga, K. A. Nguyen, S. J. Su, T. L. Windus, M. Dupuis, and J. A. Montgomery, J. Comput. Chem. **14**, 1347 (1993).